KSME

Springer

Journal of Mechanical Science and Technology 35 (5) 2021

Original Article
DOI 10.1007/s12206-021-0435-1

Keywords:
· Convex optimization
· Dynamic model identification
· Excitation trajectory
· Force estimation
· Industrial robots

Correspondence to:
Omer Faruk Argin
oargin@itu.edu.tr

Citation:
Argin, O. F., Bayraktaroglu, Z. Y. (2021). Consistent dynamic model identification of the Stäubli RX-160 industrial robot using convex optimization method. Journal of Mechanical Science and Technology 35 (5) (2021) 2185~2195.
http://doi.org/10.1007/s12206-021-0435-1

Received September 25th, 2020
Revised February 3rd, 2021
Accepted February 22nd, 2021

† Recommended by Editor
Ja Choon Koo

Consistent dynamic model identification of the Stäubli RX-160 industrial robot using convex optimization method

Omer Faruk Argin[1] and Zeki Yagiz Bayraktaroglu[2]

[1]Mechatronics Eng. Dept., Istanbul Technical University, Istanbul, Turkey, [2]Mechanical Eng. Dept., Istanbul Technical University, Istanbul, Turkey

Abstract Dynamic models of robot manipulators with standard dynamic parameters are required for simulations, model-based controller design and external force estimation. The aim of this work is to identify the complete dynamic model of the 6-axis Stäubli RX-160 industrial robot. A convex optimization-based method is used for parameter identification. Consistent model parameters are obtained as the result of the optimization procedure subject to physical constraints. Low-speed behavior of the robot being dominated by joint friction, the dynamic model includes an algebraic friction model consisting of the Coulomb and viscous friction components along with the Stribeck effect. The coupled mechanical structure of the 5th and 6th joints, and elasticity due to the presence of balancing springs are also represented in the proposed dynamic model. The ordinary least square error method is used for the performance evaluation of the convex optimization-based method. Estimated parameters from both methods are experimentally verified over identification and test trajectories. The identified model is finally used as a basis in the estimation of external forces acting on the robot's end-effector. The proposed sensor-less model-based approach for the estimation of external forces constitutes an alternative mean of experimental validation. Comparison of computed external forces with measured ones by an F/T transducer shows that the dynamic model obtained with the proposed method provides an accurate estimation.

1. Introduction

Many robotic applications such as machining, welding or surgical operations require high performances in terms of trajectory tracking with high accuracy and repeatability. In this context, design of advanced controllers, for both motion and force control applications, are based on the robot dynamic models and their performances depend largely on the model accuracy [1-3]. Realistic simulation of robot manipulators require also the knowledge of precise dynamic models, e.g., in surgical training simulators [4]. Furthermore, in model based controller design, tuning of control parameters becomes easier in presence of precise dynamic models. Introduction of poor dynamic models in the control loops results in higher controller gains, which in turn amplify disturbances.

High precision modelling necessitate a comprehensive approach for the establishment of the dynamic equations, as well as accurate model parameters. Robot manufacturers generally do not or only partly provide the dynamic model parameters. In general, these parameters turn out to be inaccurate for each individual robot because of the complexity of friction characteristics, disparities in manufacturing and assembly or operational conditions. Since dynamic parameters are not directly measurable, their identification is of great importance and constitutes an interesting research topic [5-7].

The procedure of experimental parameter identification involves the modelling, exciting trajectory generation, measurement, signal processing, parameter estimation, and model validation, where the exciting trajectory design and parameter estimation methods mainly affect the identification accuracy [5]. In order to improve the parameter estimation speed and reduce the

sensitivity to actuator and measurement noise, trajectories used in the experiments must be carefully generated. Furthermore, the generated trajectories should also excite all dynamic properties of the robot. Experiments show that intuitively chosen trajectories are likely to provide poor excitation.

Generation of sufficiently exciting trajectories can be achieved by an optimization procedure. The condition number of the regression matrix which improves the measurement's signal-to-noise ratio is proposed to optimize the exciting trajectory [8]. Researchers mostly use finite Fourier series trajectory generation methods based on the minimum condition number of the coefficient matrix of the linearized dynamic equation [9, 10]. Since the Fourier series are periodical, this method results in the continuous repetition of the trajectory and therefore the average filtered data improves the measurement's signal-to-noise ratio.

Numerical optimization methods are used to estimate dynamic model parameters from measured data recorded during experiments. The ordinary least squares (OLS) method [11], weighted least squares (WLS) method [12], maximum likelihood estimation (MLE) method [13] and Kalman filter method [14] are commonly used approaches. A basic neural network [15], a modified genetic algorithm [16], a fuzzy adaptive differential evolution algorithm [17], artificial fish swarm [18], particle swarm [19] and deep learning [6] are among artificial intelligence based identification methods presented in literature.

In practice, identification techniques cannot always guarantee the estimation of physically feasible solutions [20]. The physical feasibility conditions are related to constraints such that the kinetic energy and inertia tensor must be positive definite, or that the sum of any two of the eigenvalues of the inertia tensor must be larger than the third one [21]. These constraint problems are usually treated within the linear matrix inequality (LMI) with semi-definite programming (SDP) framework technique [22]. Experimental results show that the enforcement of the physical feasibility constraints can improve overfitting [23]. Iteratively reweighted least squares (IRLS) [24], penalty-based optimization [7], and a universally global optimization methods [25] are proposed in order to obtain physically feasible model parameters.

Convex optimization can be considered as a generalization of both least-squares and linear programming approaches. Advantages of the convex optimization are that, a convex feasible region makes it easier to ensure that infeasible solutions are prevented while searching for an optimum in a constrained problem, and in conjunction with a convex feasible region, a convex objective function ensures that all local optima are global [26]. Therefore, reflecting prior knowledge about the system in terms of constraints to be satisfied in the least-squares formulation, the convex optimization reduces the uncertainties in parameter estimation [27].

Joint friction is also one of the important source of dynamic forces and should be modeled and identified adequately. The basic algebraic friction models include the Coulomb and viscous effects, and the extended models are proposed by the consideration of static friction as an additional effect [28-30].

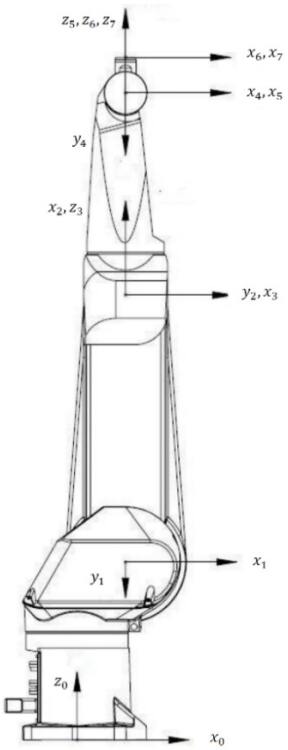

Fig. 1. Coordinate frames of the Stäubli RX160.

More complex static friction models involve the Stribeck effect, dominant at low speeds [31].

Performances of robot controllers, designed for fast and accurate tasks, are deteriorated by external forces acting as physical disturbances. Real-time perception of external forces and their consideration in controller design improve the closed-loop performances [30]. Additional F/T sensors are required to measure the external forces acting on the end-effector for proper force feedback to the local environment. However, it might be either technically difficult to mount such sensors or too expensive, according to the application.

In this study, a sensor-less model-based method is proposed for the estimation of the external end-effector forces when the robot interact with the environment. The joint torques of the robot, computed through of the identified dynamic model, are subtracted from the measured joint torques in order to obtain the additional torques due to the external interaction. The wrench at the end-effector is calculated by means of the inverse transpose of the Jacobian matrix. This approach has been used in different robotic systems [32-34]. The method proposed in this paper can be regarded as an extension of Refs. [32, 33], with the consideration of a complex friction model and joint torques due to the external interaction.

The main goal of this work is to identify a consistent dynamic model of the Stäubli RX-160 industrial robot (Fig. 1) as a case study. The base parameters, defined in a linear parameter vector of minimal order [35, 36], are used in the modeling equations of the robot. Base parameters are linear combinations of the dynamic parameters of each link composing the

robot and their use results in a well-conditioned over-determined regression matrix. A friction model including the complex Stribeck effect is used and the mechanical coupling between the 5th and 6th joints of the robot is taken into account in order to establish a realistic dynamic model.

A convex optimization algorithm dealing with linear, nonlinear and conditional constraints is applied to obtain the consistent dynamic model parameters. In order to minimize the impact of measurement noise, optimal exciting trajectories are also generated within the convex optimization framework. The dynamic model obtained by the proposed method is validated through experimental analysis with the investigation of the sensor-less model-based external force estimation. The identified model is also compared to the one obtained by the ordinary least squares method.

The rest of the article is arranged as follows: In Sec. 2, kinematics and dynamics of the Stäubli RX-160 robot is introduced. Sec. 3 presents the identification method for the dynamic parameters. In Sec. 4, calculation of the optimal excitation trajectory is presented. Experimental results are given and discussed in Sec. 5. Sec. 6 gives the conclusion.

2. Kinematic and dynamic modeling of the Stäubli RX160 robot

2.1 Kinematics

Geometrical modeling of robots can be achieved by the Denavit-Hartenberg (DH) formulation based on kinematic frames located on the joint axes. The Stäubli RX160 is equipped with 6 revolute joints. The first four joints of the robot are directly driven by servo motors via helical gear transmissions as shown in Fig. 2. For the remaining two joints, the servos are mounted inside the fourth link of the robot and a gear transmission transfers the motion from servo 6 through the 5th joint to the 6th joint [37]. This mechanical design causes a kinematic coupling between the servo 5 and joint 6 as shown in Fig. 3. The angular velocity of servo 6 is related to the difference of joint velocities $\dot{q}_5$ and $\dot{q}_6$. Consequently, one needs to define additional coordinate axes in order to take into account this extra friction model. The velocity $\dot{q}_7$ associated with the additional coordinate axes is defined as follows:

$$\dot{q}_7 = \dot{q}_5 + \dot{q}_6 . \tag{1}$$

The frame definition of the robot is shown in Fig. 1, and the corresponding DH parameters in Table 1. For each link in the Table 1, the transformation matrix T_{i-1}^{i} of the frame attached to the link i with respect to the frame attached to link $i-1$ can be given as follows:

$$T_{i-1}^{i} = \begin{bmatrix} c\theta_i & -s\theta_i c\alpha_i & s\theta_i s\alpha_i & a_i c\theta_i \\ s\theta_i & c\theta_i c\alpha_i & -c\theta_i s\alpha_i & a_i s\theta_i \\ 0 & s\alpha_{ii} & c\alpha_i & d_i \\ 0 & 0 & 0 & 1 \end{bmatrix} \tag{2}$$

Table 1. DH parameters of the Stäubli RX160.

Frame	a_i	α_i	d_i	θ_i
1	a_1	$-\pi/2$	d_1	θ_1
2	0	0	d_2	$\theta_2 - \pi/2$
3	0	$\pi/2$	0	$\theta_3 + \pi/2$
4	a_4	$-\pi/2$	0	θ_4
5	0	$\pi/2$	0	θ_5
6	a_6	0	0	θ_6

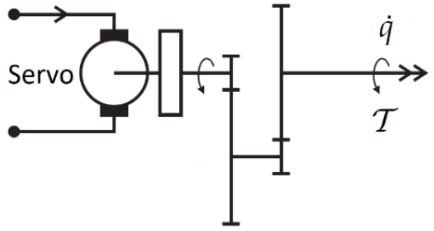

Fig. 2. Schematic overview of the joints 1-4 assembly [36].

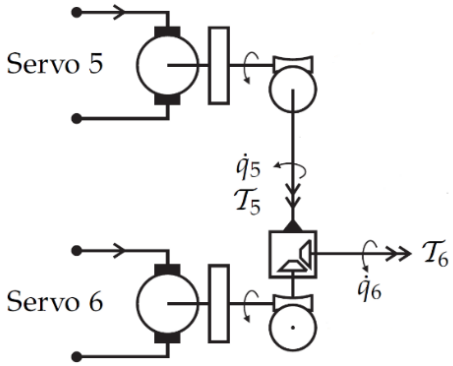

Fig. 3. Schematic overview of the joints 5 and 6 assembly [36].

where $c\theta_i$ and $s\theta_i$ are the standard abbreviations of $\cos(\theta_i)$ and $\sin(\theta_i)$.

2.2 Dynamics

The basic equations of motion are derived by using the Euler-Lagrange equations [38]. The Lagrangian function is defined as the difference between the kinetic energy T and potential energy V of the robot, $L = T - V$. Then, the Euler-Lagrange equations are expressed as follows:

$$\frac{d}{dt}\left(\frac{\partial L}{\partial \dot{q}_i}\right) - \frac{\partial L}{\partial q_i} = \tau_i \quad \text{for} \quad i = 1, 2, ...n \tag{3}$$

where the joint variables q_i represent the generalized coordinates, and $\boldsymbol{\tau}_i$ the scalar joint torques. One can obtain the dynamic model of a n-DOF robot in standard form as follows:

$$M(\boldsymbol{q})\ddot{\boldsymbol{q}} + \boldsymbol{b}(\boldsymbol{q}, \dot{\boldsymbol{q}}) + \boldsymbol{g}(\boldsymbol{q}) + \boldsymbol{\tau}_s(\boldsymbol{q}) + \boldsymbol{\tau}_f(\dot{\boldsymbol{q}}) = \boldsymbol{\tau} + \boldsymbol{\tau}_e \tag{4}$$

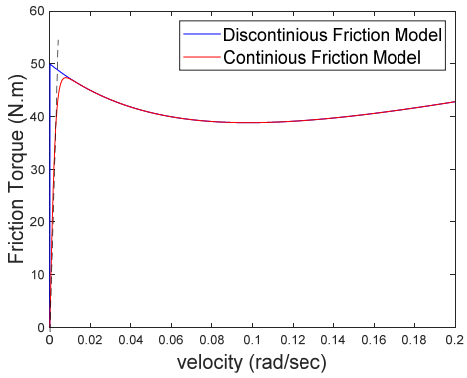

Fig. 4. Positive velocity joint friction model with static, viscous, Coulomb friction and Stribeck effect.

where $\boldsymbol{q},\dot{\boldsymbol{q}},\ddot{\boldsymbol{q}}\epsilon R^6$ represent, respectively, the joint positions, velocities and acclerations. $M(\boldsymbol{q})\epsilon R^{6\times6}$ is the inertia matrix, $\boldsymbol{b}(\boldsymbol{q},\dot{\boldsymbol{q}})\epsilon R^6$ is the vector of the Coriolis and centrifugal forces, $\boldsymbol{g}(\boldsymbol{q})\epsilon R^6$ the vector of gravitational forces, $\boldsymbol{\tau}_s(\boldsymbol{q})\epsilon R^6$ the torque vector due to the balancing spring system, $\boldsymbol{\tau}_f(\dot{\boldsymbol{q}})\epsilon R^6$ the friction torque vector, $\boldsymbol{\tau}_e\epsilon R^6$ the torque vector due to the external interaction with environment and $\boldsymbol{\tau}\epsilon R^6$ represents the input joint torque vector.

Joint friction must be considered in order to establish a complete model of the manipulator. Although joint friction happens to be a highly complex physical phenomenon, one of the comprehensive classical models in Ref. [39], which is the combination of viscous, static and Coulomb friction along with the Stribeck effect, is generally used for its description:

$$\boldsymbol{\tau}_{fr}(\dot{\boldsymbol{q}})=\left[F_c+(F_s-F_c)e^{-|\dot{q}/\dot{q}_s|}\right]\mathrm{sgn}(\dot{\boldsymbol{q}})+F_v\dot{\boldsymbol{q}} \tag{5}$$

where $\boldsymbol{\tau}_{fr}(\dot{\boldsymbol{q}})\epsilon R^6$ is a known nonlinear discontinuous friction model torque, $F_c\epsilon R^6$ is the Coulomb friction coefficient, $F_s\epsilon R^6$ is the stiction force coefficient, $\dot{\boldsymbol{q}}_s\epsilon R^6$ is the Striebeck velocity and $F_v\epsilon R^6$ is the viscous friction coefficient. This model is discontinuous as shown in Fig. 4. In order to achieve sensitivity to quantization errors, measurement noise and the sudden jump of friction compensation at zero velocity, the discontinuous friction model Eq. (5) is approximated by the following continuous function (also shown in Fig. 4):

$$\boldsymbol{\tau}_f(\dot{\boldsymbol{q}})=2/\pi\arctan(\boldsymbol{c}\dot{\boldsymbol{q}})\boldsymbol{\tau}_{fr}(\dot{\boldsymbol{q}}) \tag{6}$$

where parameter $c\epsilon R^6$ is a scaling constant.

In the Stäubli RX-160, a spring is mounted along the second link to compensate for the gravitational torque acting on the second joint. The elastic contribution $\boldsymbol{\tau}_s$ models the spring forces acting on joint 2. These torques can be modeled as follows:

$$\boldsymbol{\tau}_s(\boldsymbol{q})=K\boldsymbol{q} \tag{7}$$

where $K=diag[0,k,0,0,0,0]\epsilon R^{6x6}$ is the stiffness constant.

The external joint torques ($\boldsymbol{\tau}_e(\boldsymbol{q})$) originate from the external force applied to the robot. If it is assumed that all external forces are applied to the end-effector of the robot, then the external joint torque vector is computed as follows:

$$\boldsymbol{\tau}_e(\boldsymbol{q})=J^TF \tag{8}$$

where $J\epsilon R^{6\times6}$ the Jacobian matrix of the robot, and $F\epsilon R^6$ denotes the generalized force vector applied to the end-effector.

3. Identification of dynamic parameters

Identification of the dynamic parameters of the robot is based on the property of linearity of the dynamic model with respect to a suitable set of dynamic parameters, known as barycentric parameters [38]. In this approach, all the parameters of the dynamic model appearing in Eq. (4) are represented in a vector $\boldsymbol{\delta}$. For an 6-DOF manipulator, the vector $\boldsymbol{\delta}$ contains the following unknown parameters for $i=1,..,6$:

- m_i : the mass of the link i,
- $l_i:\left[l_i^x,l_i^y,l_i^z\right]$ the three components of the center of mass (COM) relative to the link frame i,
- $I_i:\left[l_i^{xx},l_i^{yy},l_i^{zz},l_i^{xy},l_i^{xz},l_i^{yz}\right]$ the six independent components of the inertia tensor about the frame i,
- k_i the spring constant about the frame i,
- $F_{c_i},F_{s_i},F_{v_i},q_{s_i},c_i$ the five friction coefficients about the frame i.

Consequently, each robot link has the following 16 parameters:

$$\boldsymbol{\delta}_i=\left[m_i,l_i^x,l_i^y,l_i^z,l_i^{xx},l_i^{yy},l_i^{zz},l_i^{xy},l_i^{xz},l_i^{yz},k_i,F_{c_i},F_{s_i},F_{v_i},q_{s_i},c_i\right]. \tag{9}$$

Then, the dynamic model of the robot can be rearranged in a parameter linear form as follows:

$$\boldsymbol{\tau}=\mathrm{Y}(\boldsymbol{q},\dot{\boldsymbol{q}},\ddot{\boldsymbol{q}})\boldsymbol{\delta} \tag{10}$$

where $\boldsymbol{\delta}\epsilon R^{96}$ is the vector of unknown parameters and $\gamma\epsilon R^{6\times96}$ represents the regression matrix. The regression matrix γ is a function of the joint positions, velocities and accelerations.

All the parameters do not explicitly appear in the dynamic model Eq. (10) and some of them are identifiable only as linear combinations of other parameters [40]. There are also some parameters that are unidentifiable due to the mechanical structure of the manipulator. Therefore, a reduced vector of base parameters is obtained by a numerical decomposition of the regression matrix γ [40]:

$$\boldsymbol{\tau}=\gamma_b(\boldsymbol{q},\dot{\boldsymbol{q}},\ddot{\boldsymbol{q}})\boldsymbol{\delta}_b \tag{11}$$

where $\gamma_b = \gamma P, \epsilon R^{6\times57}$ is a matrix and $\boldsymbol{\delta}_b = P^T\boldsymbol{\delta}, \epsilon R^{57}$ is the of barycentric parameters. Hence, $P\epsilon R^{96\times57}$ represents the permutation matrix.

In the identification, the excitation trajectories described in the following section are used as motion references of the robot. While the robot moves over these trajectories, the joint positions and torques are recorded at the sampling times $t_1,\ldots,t_m$. Then the dynamic regression matrix is written as follows:

$$\boldsymbol{\beta} = \begin{bmatrix} \boldsymbol{\tau}(t_1) \\ \boldsymbol{\tau}(t_2) \\ \vdots \\ \boldsymbol{\tau}(t_m) \end{bmatrix} = \begin{bmatrix} \gamma_b\left(\boldsymbol{q}(t_1),\dot{\boldsymbol{q}}(t_1),\ddot{\boldsymbol{q}}(t_1)\right) \\ \gamma_b\left(\boldsymbol{q}(t_2),\dot{\boldsymbol{q}}(t_2),\ddot{\boldsymbol{q}}(t_2)\right) \\ \vdots \\ \gamma_b\left(\boldsymbol{q}(t_m),\dot{\boldsymbol{q}}(t_m),\ddot{\boldsymbol{q}}(t_m)\right) \end{bmatrix} \cdot \boldsymbol{\delta}_b = W\boldsymbol{\delta}_b \tag{12}$$

where the indices ($i = 1,\ldots, m$) represent the sampling instants. Then, $\boldsymbol{\beta}\epsilon R^{6\times m}$ represents the torque matrix, $W\epsilon R^{6\times57}$ represents the regression matrix and $\boldsymbol{q}$ are the joint coordinate at sampling times.

The identification is achieved through the minimization of an objective function which minimizes the squared residual error ($\boldsymbol{\epsilon} = \boldsymbol{\Gamma} - \boldsymbol{\beta}$) with respect to the decision vector $\boldsymbol{\beta}$. The constrained optimization problem is then expressed as follows:

$$minimize \left|\left|\boldsymbol{\Gamma} - \boldsymbol{\beta}\right|\right|^2 \ subject\ to\ \boldsymbol{\delta}_b = P^T\boldsymbol{\delta} \tag{13}$$

where $\boldsymbol{\Gamma}$ is the vector of measured joint torque, $\boldsymbol{\beta} = W\boldsymbol{\delta}_b$ is the calculated torque vector. Both the existence domain D of the vector $\boldsymbol{\delta}$ and the objective function are expressed in a linear matrix inequality (LMI) form, suitable for semi-definite programming techniques.

The ordinary least squares (OLS) method is also applied in the identification. The parameters obtained by the OLS method is used as a basis of comparison for the results of the convex optimization based parameter estimation. Since the OLS method does not involve constraints, the optimization criterion used for the OLS method can be expressed as follows:

$$minimize \left|\left|\boldsymbol{\Gamma} - \boldsymbol{\beta}\right|\right|^2. \tag{14}$$

3.1 Definition of the constraints

The identified barycentric parameter vector $\boldsymbol{\delta}_b$ might be possibly physically unfeasible in cases such that the estimation of negative values for inertia. In order to obtain consistent parameters and avoid overfitting to the identification data, physical constraints on the dynamic parameters for each link i are defined as follows:

- The mass m_i must be positive between the lower and upper bound : $0 < m_{i_{min}} \le m_i \le m_{i_{max}}$.
- The inertia eigenvalues σ_x, σ_y and σ_z must satisfy the triangle inequality condition: $\sigma_x + \sigma_y > \sigma_z, \sigma_y + \sigma_z > \sigma_x$, and $\sigma_x + \sigma_z > \sigma_y$ [7].
- The center of mass must remain inside its convex hull: $m_i r_{l_i} - l_i \le 0$ and $m_i r_{ui} + l_i \le 0$, where r_{li} and r_{ui} are the lower and upper bounds of l_i, respectively [31].
- The viscous, static, Coulomb friction coefficients and the Stribeck velocity for each joint i have upper and lower bounds.
- The stiffness of the spring is strictly positive: $k_i > 0$.

4. Optimal trajectory generation

In order to generate sufficiently rich trajectories, the problem of trajectory generation can be redefined as an optimization problem. The condition number of the regression matrix W is a measure of the sensitivity of the solution $\boldsymbol{\delta}_b$ with respect to the errors on $\boldsymbol{\Gamma}$ and W [10]. Therefore, the problem of the optimal trajectory generation is expressed as searching suitable values in a constrained domain by minimizing the condition number of the regression matrix. The objective function is given as follows:

$$minimize\ cond(W),$$

as proposed in Ref. [9], the trajectory of the i^{th} joint can be rewritten in terms of sinusoidal components as follows:

$$q_i(t) = q_{i0} + \sum_{i=1}^{n} \frac{a_l^i}{w_f l}\sin\left(w_f lt\right) + \frac{b_l^i}{w_f l}\cos\left(w_f lt\right) \tag{15}$$

where $w_f = 2\pi f_f$ is the fundemental frequency and n is the number of the Fourier series harmonics, a_l^i, b_l^i are the amplitudes of the n^{th} order triganometric functions and q_{i0} is the initial joint positions, then, for n harmonic component in Eq. (15), there are $2n+1$ unknowns, i.e., the dynamic parameters per joint to be identified by optimization.

The selection of the trajectory should satisfy the boundary conditions, and the minimum number of conditions of the regression matrix W. In this work, constraints on the joint variables, i.e., position, velocity and acceleration, and task space position, are applied as follows:

- $q_{i\min} \le q_i \le q_{i\max}$;
- $\dot{q}_{i\min} \le \dot{q}_i \le \dot{q}_{i\max}$;
- $\ddot{q}_{i\min} \le \ddot{q}_i \le \ddot{q}_{i\max}$;
- $x_{i\min} \le x_i \le x_{i\max}$.

Finally, the convex optimization method is applied to solve this constrained nonlinear optimization problem.

5. Experiments

This section presents the experimental procedures and results of the dynamic model identification of the Stäubli RX-160

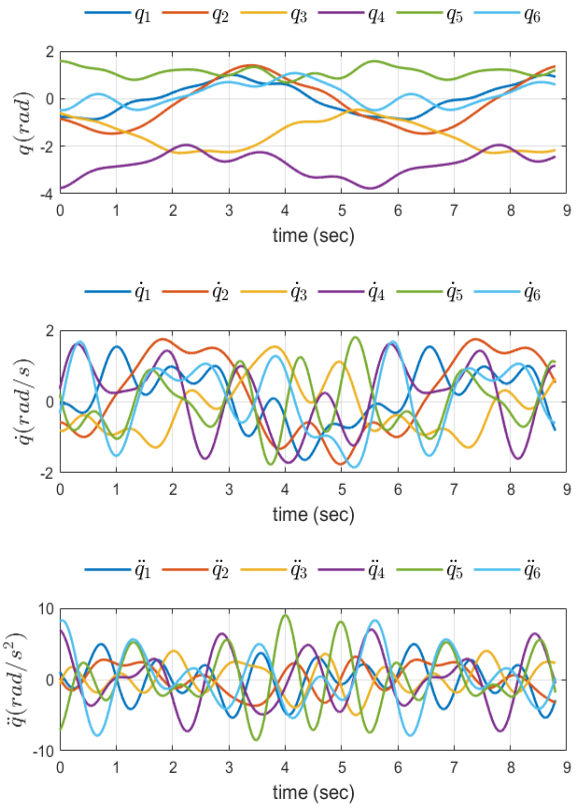

Fig. 5. Position, velocity and acceleration profiles of the optimal identification trajectory.

robot introduced in Sec. 3. A 6-axis ATI Delta SI 660-60 F/T transducer is mounted on end-effector of the robot in order to verify the calculated external force of the robot. The controllers are implemented through the low level interface (LLI) provided in Ref. [41]. The LLI provides the user with the joint position, velocity and torque feedback and includes two control modes: in position-velocity and in torque. The position control mode is used in this work.

5.1 Trajectory generation

In the first step, the optimal excitation trajectories are obtained by solving the trajectory optimization problem for all joints. The fundamental frequency is $w_f = 0$, 1 and the number of Fourier series harmonics is $n = 6$ as trigonometric trajectory paramters in Eq. (15). Physical constraints on the joints are applied within their and environment ranges in the optimization (Tables 2 and 3). Convex optimization method is applied by using the CVXPY package with SCS solver [42]. The optimal excitation trajectories shown in Fig. 5, in terms of the joint position, velocity and acceleration, are generated within the joint limits given in Tables 2 and 3.

5.2 Model identification

In the second step, robot is operated in position-velocity control mode according to the optimal excitation trajectories and motion data is collected synchronously. While the joint position, velocity and torque are measured at the sampling frequency of 250 Hz, the joint acceleration is computed by the second-order numerical differentiation of the velocity.

Since the measured velocities and torques, and computed accelerations are highly noisy, all the signals are filtered using a Kalman filter. The CVXPY package is then used for the iden-

Table 2. Position, velocity and acceleration constraints per joints.

i	Pos. (rad)		Vel. (rad/sec)		Acc. (rad/sec^2)	
	Min	Max	Min	Max	Min	Max
1	-2.78	2.78	-3.49	3.49	-7.9	7.9
2	-1.5	1.5	-3.49	3.49	-6.5	6.5
3	-2.5	2.5	-4.45	4.45	-10.5	10.5
4	-4.0	4.0	-5.50	5.50	-25.2	25.2
5	-1.75	1.75	-6.80	6.80	-19.6	19.6
6	-4.40	4.40	-15.18	15.18	-41.7	41.7

Table 3. Task space constraints of the robot.

	$x(m)$	$y(m)$	$z(m)$
Min	-2.11	-0.5	0.55
Max	2.11	1.5	2.11

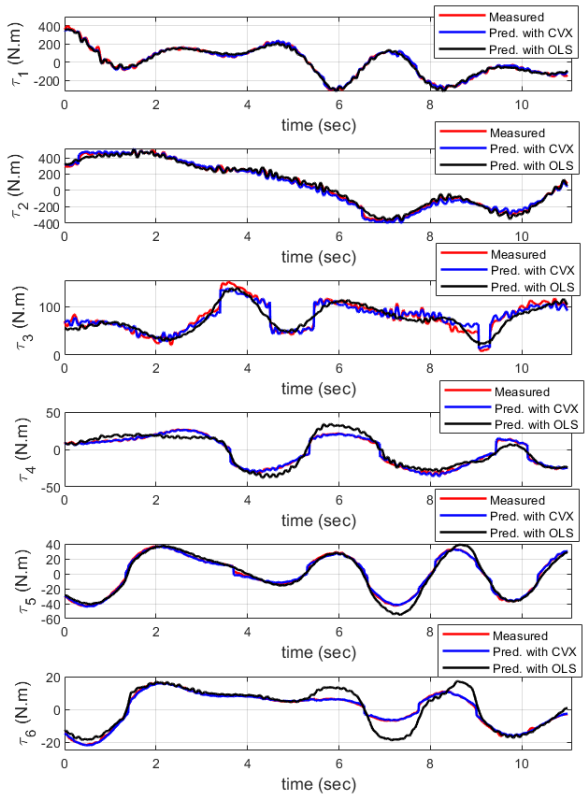

Fig. 6. Measured and predicted joint torques over the optimal identification trajectory.

Table 4. Identified dynamic parameters of the Stäubli RX-160 robot.

	Opt\Frame	1	2	3	4	5	6	7
m_i	CVX	54.332	39.966	10.007	10.013	0.686	0.103	0.0
	OLS	156e+11	741e+10	-565e+10	-811e+9	139e+10	676e+10	0.0
l_i^x	CVX	-0.150	-0.122	-0.158	4.8e-5	0.107	-0.050	0.0
	OLS	-2.891	0.0	0.0	0.0	0.0	0.0	0.0
l_i^y	CVX	0.0	0.699	-0.300	-0.039	-0.049	0.097	0.0
	OLS	0.529	-0.26	-0.394	-2.432	-1.419	0.0	0.0
l_i^z	CVX	7e-7	-0.699	0.299	-0.122	0.105	0.074	0.0
	OLS	-1.072	-1.01	1.861	-7.313	-16.192	3.219	0.0
I_i^{xx}	CVX	0.216	48.358	8.646	3.032	0.308	0.657	0.0
	OLS	-223e+11	443e+10	215e+11	508e+11	-371e+12	-733e+11	0.0
I_i^{yy}	CVX	0.0	-0.246	-2.022	-0.181	-0.085	-0.053	0.0
	OLS	-884e+10	8.047	-4.082	-3.308	-1.188	1.077	0.0
I_i^{zz}	CVX	3e-4	-9.813	-1.212	2.102	0.350	0.249	0.0
	OLS	494e+11	-12.028	-1.566	2.267	1.173	1.077	0.0
I_i^{xy}	CVX	0.215	46.790	3.924	4.440	0.716	0.684	0.0
	OLS	-159e+12	-141e+10	941e+10	433e+11	-366e+12	-733e+10	0.0
I_i^{xz}	CVX	0.0	-3.710	0.609	0.261	0.069	0.172	0.0
	OLS	-370e+10	221e+10	415e+10	-144e+11	319e+11	-0.945	0.0
I_i^{yz}	CVX	-0.012	6.091	11.025	1.442	0.435	0.212	0.0
	OLS	-139e+12	584e+11	121e+11	753e+10	-553e+10	0.711	0.0
k_i	CVX	0.0	0.012	0.0	0.0	0.0	0.0	0.0
	OLS	0.0	-11892.642	0.0	0.0	0.0	0.0	0.0
F_{c_i}	CVX	36.015	60.694	25.181	9.041	5.535	0.254	1.307
	OLS	78.596	91.918	53.838	19.012	3.172	-1.772	3.966
F_{s_i}	CVX	3.653	-32.248	11.738	-0.366	-0.663	0.197	-0.065
	OLS	9798.862	4723.866	4637.736	497.059	303.847	187.480	-29.863
F_{v_i}	CVX	154.055	106.709	16.508	18.446	21.600	0.073	5.043
	OLS	103.097	78.488	-17.920	9.038	23.587	-0.291	4.036
q_{s_i}	CVX	0.011	0.011	0.013	0.012	0.011	0.012	0.011
	OLS	0.011	0.011	0.013	0.012	0.011	0.012	0.011
c_i	CVX	3.2	3.2	3.2	5.0	5.0	5.0	5.0
	OLS	3.0	3.0	3.0	4.2	4.2	4.2	4.2

tification of the dynamic parameters by solving the Eq. (12) based on the experimental data and the proposed model of robot dynamics. For comparison, the pyOpt package [43] is used for the identification of the unconstrained dynamic parameters with the OLS method by solving the Eq. (13) based on the experimental data and the proposed model of robot dynamics. Fig. 6 shows the comparison of the measured and predicted joint torques on the optimal identification trajectories for the convex and OLS methods in a trajectory period. The identified dynamic base parameters are given in Table 4.

5.3 Experimental validation based on test trajectories

In the third step, the identification of the dynamic model parameters is experimentally validated. The test trajectories shown in Fig. 7 are also generated by using finite Fourier series. The measured and estimated joint torques are recorded and compared to each other. Fig. 8 shows the predicted and measured torques recorded on a test trajectory.

Tables 5 and 6 show the mean of the torque prediction errors and their standard deviations for the identification trajectory and test trajectories. The residual root mean square error (RMSE) is calculated to verify the deviation of the predicted torque error. For each sample, the torque error vector is calculated as follows:

$$\boldsymbol{e}_\tau = \frac{\sqrt{\sum_{i=1}^{N}\left(\boldsymbol{\tau}_m - \boldsymbol{\tau}_p\right)^2}}{N} \tag{16}$$

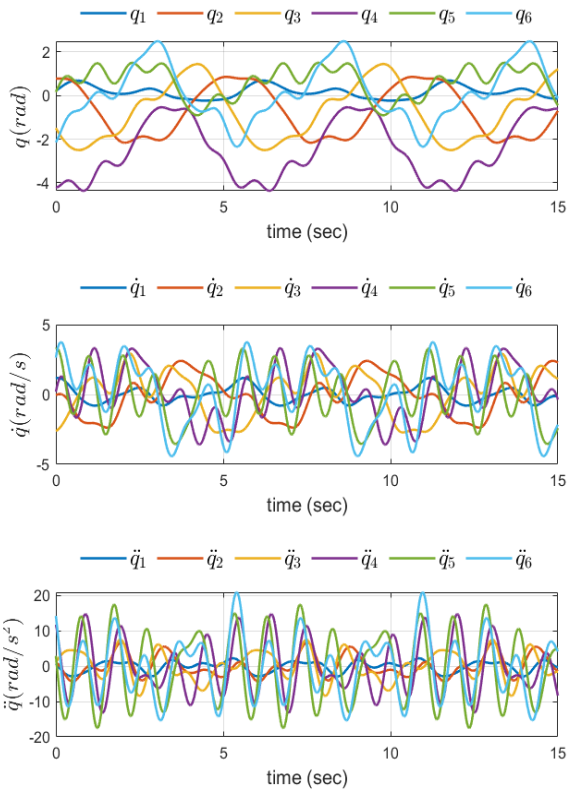

Fig. 7. Position, velocity and acceleration profiles over test trajectories.

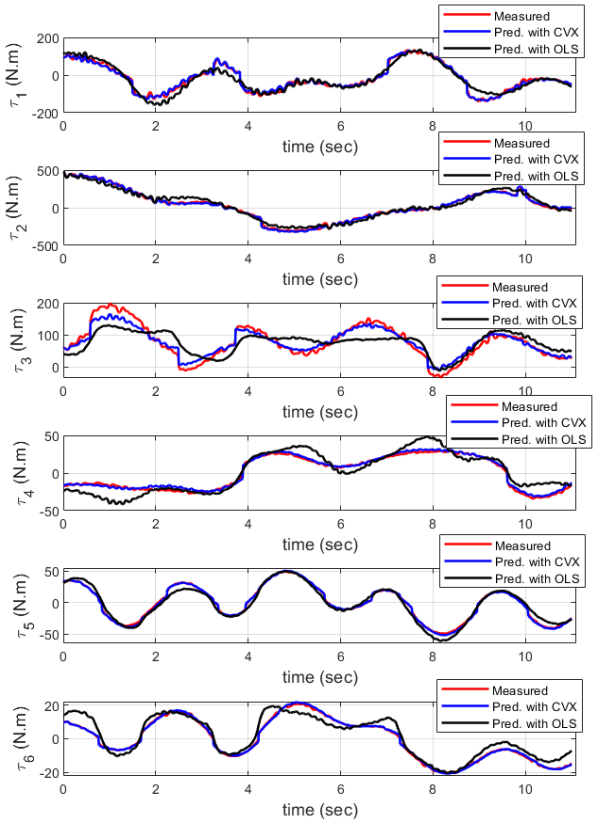

Fig. 8. Measured and predicted joint torques over the test trajectory.

Table 5. Mean of error and standard deviation for the identification trajectories with the convex optimization and OLS methods.

Joint	Convex opt.		OLS opt.	
	Mean (N.m)	Std. deviation	Mean (N.m)	Std. deviation
1	9.608	8.425	12.535	9.899
2	18.919	13.538	13.639	11.812
3	6.031	4.403	7.022	4.940
4	0.992	0.870	2.7892	1.935
5	0.987	0.745	2.024	1.622
6	0.388	0.357	1.657	1.854
Average	6.154	7.231	6.644	5.358

Table 6. Mean of error and standard deviation for the test trajectories with the convex optimization and OLS optimization methods.

Joint	Convex opt.		OLS opt.	
	Mean (N.m)	Std. deviation	Mean (N.m)	Std. deviation
1	7.209	6.07	11.456	9.1446
2	10.832	8.624	19.281	12.896
3	12.343	8.896	24.577	14.631
4	2.004	1.411	5.873	4.125
5	1.067	0.835	2.891	2.198
6	0.453	0.344	1.954	1.365
Average	5.651	5.203	11.005	9.241

where $\boldsymbol{\tau}_m$ and $\boldsymbol{\tau}_p, \epsilon R^6$ represent the measured and predicted joint torques for each sample, respectively, and N defines number of sample.

Comparison of the Tables 5 and 6 shows that the dynamic models identified with the convex optimization and OLS methods perform equally well over the identification trajectory. Although the mean errors in different joints differ from each other, the average mean error is almost equal in both cases. However, the experimental results obtained with the convex method performs largely better than the OLS method over test trajectories.

While the average mean error remains in the same order of magnitude with the convex identification, it is almost doubled with the OLS identification. Hence, the performances obtained with the realistic dynamic parameters provided by the convex optimization prove to be suitable for the control of the robot over randomly generated trajectories.

5.4 Experimental validation based on the estimation of external forces

In the fourth step, estimation of the external forces acting on the end-effector is considered as an additional mean of experimental validation. The dynamic model identified here is used to estimate the external forces in two experiments. External forces are measured by the 6-axis ATI delta F/T transducer.

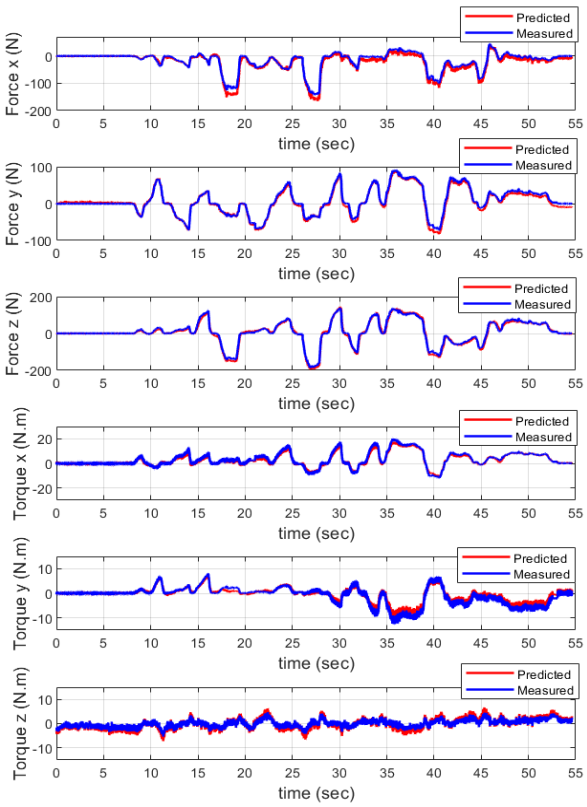

Fig. 9. The measured and predicted wrench at the end-effector for a load manipulation.

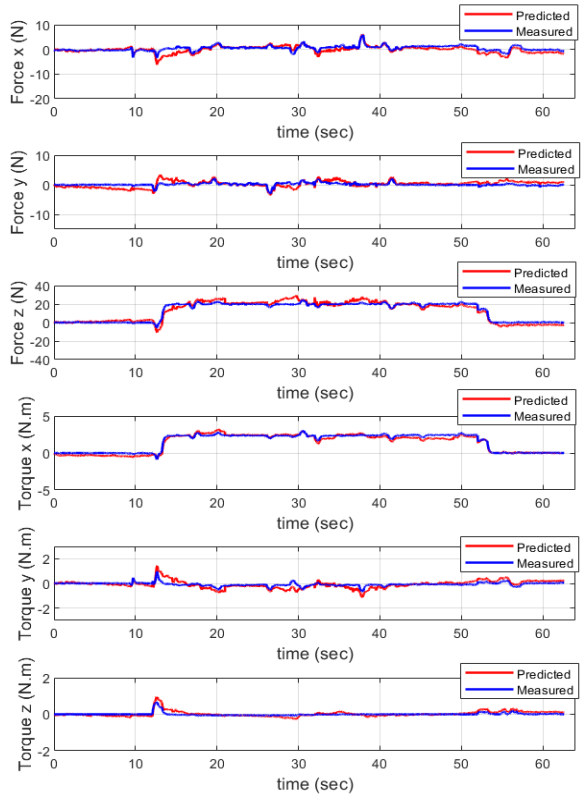

Fig. 10. The measured and predicted wrench at the end-effector.

Table 7. Mean of error and standard deviation of the estimated force/torque values.

	1st experiment (manually applied externalforce)			2nd experiment (external forces due to object manipulation)		
	Mean error	Std. dev.	e_{RAE}	Mean error	Std. dev.	e_{RAE}
F_x (N)	13.81	12.89	1.243	0.78	0.65	1.195
F_y (N)	19.28	13.07	0.565	0.73	0.52	0.752
F_z (N)	12.43	10.13	0.416	2.36	1.61	1.418
M_x (N.m)	1.47	1.30	0.484	0.21	0.18	0.14
M_y (N.m)	1.42	1.29	0.796	0.17	0.13	0.643
M_z (N.m)	0.8	0.57	1.339	0.09	0.07	0.01

Kalman filters are implemented to filter out measurement noises on the force, velocity and acceleration signals. The relative absolute error between the measured and estimated signals is defined as follows:

$$\boldsymbol{e}_{RAE} = \frac{\sum_{i=1}^{N} \left| \boldsymbol{F}_m - \boldsymbol{F}_p \right|}{\sum_{i=1}^{N} \left| \boldsymbol{F}_m - \boldsymbol{F}_{ma} \right|} \tag{17}$$

where $\boldsymbol{F}_m$ and $\boldsymbol{F}_v$ represent, respectively, the measured and predicted end-effector force and $\boldsymbol{F}_{ma}$ is the average of the measured F/T values and N the number of the samples.

In the first experiment, random external forces are manually applied to the robot's end-effector by a human-operator during the robot motion. The measured and predicted F/T values are given in Fig. 9.

In the second experiment, the robot is programmed to pick a load and release it during its motion. The measured and predicted F/T values are given in Fig. 10. At the 13th seconds of the motion, the robot picks a 2 kg load from the ground and at the 54th seconds, the load is released. Table 7 shows the error, standard deviation and relative absolute error of the predicted values from the measured ones observed in both experiments.

6. Conclusions

This paper presents the identification of the dynamic parameters of an industrial manipulator through the convex optimization method. It includes the dynamic modeling of the robot, the generation of optimal excitation trajectories for identification purpose and finally the identification of dynamic parameters with both convex optimization and OLS methods.

The study has focused on the problem of identification of consistent parameters that characterizes the dynamics of the Stäubli RX-160 robot. The Lagrangian approach is applied in the modeling the robot dynamics. The minimum number of parameters required to compute the complete dynamics of the robot has been determined. The Fourier series-based trajecto-

ries are used to excite the robot, with the condition number of the regression matrix minimized. Dynamic parameters of the robot and optimal trajectory parameters are identified by using a convex optimization based algorithm, which takes into account several constraints including the physical bounds on parameters and the triangle inequalities of the link inertia tensors.

The proposed identification framework and resulting dynamic parameters have been validated through comparisons with the parameters identified by the unconstraint OLS error optimization method. The identified dynamic parameters are also experimentally validated with the motion of the robot over test trajectories. Experimental evaluations show that the parameters identified by the convex optimization method prove to be realistic with respect to those identified by the OLS method. Application of the proposed parameters in motion control results in consistent performance over randomly generated trajectories. A major feature of the proposed framework is that additional constraints can be easily defined to be included in the optimization problem.

The dynamic model identified in this work has also been used in the estimation of external forces acting on the end-effector of the robot while in physical interaction with the environment. Thus, a sensor-less model-based method is proposed in order to estimate the external end-effector forces for force control applications of the manipulator.

The modeling and identification framework proposed here can be used to identify alternative dynamic friction models, e.g., the LuGre model. Finally, the proposed method constitutes a basis for the simulation and model-based control of industrial manipulators.

References

[1] Y. Chen, G. Ma, S. Lin and J. Gao, Adaptive fuzzy computed-torque control for robot manipulator with uncertain dynamics, *International Journal of Advanced Robotic Systems*, 9 (6) (2012) 237-245.

[2] F. Ficuciello, L. Villani and B. Siciliano, Variable impedance control of redundant manipulators for intuitive human-robot physical interaction, *IEEE Transactions on Robotics*, 31 (4) (2015) 850-863.

[3] J. Wu, X. Han and Y. Tao, Kinematic response of industrial robot with uncertain-but-bounded parameters using interval analysis method, *Journal of Mechanical Science and Technology*, 33 (1) (2019) 333-340.

[4] F. Richter, R. K. Orosco and M. C. Yip, Open-sourced reinforcement learning environments for surgical robotics, *arXiv Preprint,* arXiv: 1903.02090 (2019).

[5] W. Wu, S. Zhu, X. Wang and H. Liu, Closed-loop dynamic parameter identification of robot manipulators using modified Fourier series, *International Journal of Advanced Robotic Systems*, 9 (1) (2012) 29-37.

[6] S. Wang, X. Shao, L. Yang and N. Liu, Deep learning aided dynamic parameter identification of 6-DOF robot manipulators, *IEEE Access*, 8 (2020) 138102-138116.

[7] C. Gaz, M. Cognetti, A. Oliva, P. R. Giordano and A. De Luca, Dynamic identification of the franka emika panda robot with retrieval of feasible parameters using penalty-based optimization, *IEEE Robotics and Automation Letters*, 4 (4) (2019) 4147-4154.

[8] B. Armstrong, On finding exciting trajectories for identification experiments involving systems with nonlinear dynamics, *The International Journal of Robotics Research*, 8 (6) (1989) 28-48.

[9] J. Swevers, C. Ganseman, J. De Schutter and H. Van Brussel, Experimental robot identification using optimised periodic trajectories, *Mechanical Systems and Signal Processing*, 10 (5) (1996) 561-577.

[10] J. Jia, M. Zhang, X. Zang, H. Zhang and J. Zhao, Dynamic parameter identification for a manipulator with joint torque sensors based on an improved experimental design, *Sensors*, 19 (10) (2019) 2248-2264.

[11] S. Briot and M. Gautier, Global identification of joint drive gains and dynamic parameters of parallel robots, *Multibody System Dynamics*, 33 (1) (2015) 3-26.

[12] G. Zak, B. Benhabib, R. G. Fenton and I. Saban, Application of the weighted least squares parameter estimation method to the robot calibration, *ASME Journal of Mechanical Design,* 116 (3) (1994) 890-893.

[13] M. M. Olsen and H. G. Petersen, A new method for estimating parameters of a dynamic robot model, *IEEE Transactions on Robotics and Automation*, 17 (1) (2001) 95-100.

[14] M. Gautier and P. Poignet, Extended Kalman filtering and weighted least squares dynamic identification of robot, *Control Engineering Practice*, 9 (12) (2001) 1361-1372.

[15] W. Ge, B. Wang and H. Mu, Dynamic parameter identification for reconfigurable robot using adaline neural network, *Proc. of 2019 IEEE International Conference on Mechatronics and Automation* (2019) 319-324.

[16] K. K. Ahn and H. P. H. Anh, System modeling and identification the two-link pneumatic artificial muscle (pam) manipulator optimized with genetic algorithms, *Proc. of 2006 SICE-ICASE IEEE International Joint Conference* (2006) 4744-4749.

[17] R. D. Al-Dabbagh, A. Kinsheel, S. Mekhilef, M. S. Baba and S. Shamshirband, System identification and control of robot manipulator based on fuzzy adaptive differential evolution algorithm, *Advances in Engineering Software*, 78 (2014) 60-66.

[18] Y. Liu, Z. Hou, H. Wang, J. Liang, G. Yang, Y. Zhang, Z. Xu and W. Wang, Parameter identification of collaborative robot based on improved artificial fish swarm algorithm, *Proc. of 2020 IEEE International Conference on High Performance Big Data and Intelligent Systems* (2020) 1-7.

[19] H. Jahandideh and M. Namvar, Use of PSO in parameter estimation of robot dynamics; part two: robustness, *Proc. of IEEE 16th International Conference on System Theory, Control and Computing* (2012) 1-6.

[20] V. Mata, F. Benimeli, N. Farhat and A. Valera, Dynamic parameter identification in industrial robots considering physical feasibility, *Advanced Robotics*, 19 (1) (2005) 101-119.

[21] Y. Wang, R. Gondokaryono, A. Munawar and G. S. Fischer, A dynamic model identification package for the da Vinci re-

search kit, *IEEE Robotics and Automation Letters,* 4 (4) (2019) 3657-3664.
[22] C. D. Sousa and R. Cortesao, Physical feasibility of robot base inertial parameter identification: a linear matrix inequality approach, *The International Journal of Robotics Research*, 33 (6) (2014) 931-944.
[23] C. D. Sousa and R. Cortesao, Inertia tensor properties in robot dynamics identification: a linear matrix inequality approach, *IEEE/ASME Transactions on Mechatronics*, 24 (1) (2019) 406-411.
[24] Y. Han, J. Wu, C. Liu and Z. Xiong, An iterative approach for accurate dynamic model identification of industrial robots, *IEEE Transactions on Robotics* (2020) 1577-1594.
[25] T. Xu, J. Fan, Y. Chen, X. Ng, M. H. Ang, Q. Fang, Y. Zhu and J. Zhao, Dynamic identification of the KUKA LBR iiwa robot with retrieval of physical parameters using global optimization, *IEEE Access*, 8 (2020) 108018-108031.
[26] F. Glineur, Conic optimization: an elegant framework for convex optimization, *Belgian Journal of Operations Research, Statistics and Computer Science*, 41 (1-2) (2001) 5-28.
[27] D. Dautbegovic, Convex optimization methods for system identification, *Master's Theses*, Linnaeus University, Sweden (2014).
[28] B. Armstrong-Hélouvry, P. Dupont and C. C. De Wit, A survey of models, analysis tools and compensation methods for the control of machines with friction, *Automatica*, 30 (7) (1994) 1083-1138.
[29] H. Olsson, K. J. Åström, C. C. De Wit, M. Gäfvert and P. Lischinsky, Friction models and friction compensation, *European Journal of Control*, 4 (3) (1998) 176-195.
[30] W. Khalil and E. Dombre, *Modeling, Identification and Control of Robots,* Butterworth-Heinemann (2004).
[31] B. Bona, M. Indri and N. Smaldone, Nonlinear friction estimation for digital control of direct-drive manipulators, *Proc. of 2003 IEEE European Control Conference* (2003) 2685-2690.
[32] A. Wahrburg, S. Zeiss, B. Matthias and H. Ding, Contact force estimation for robotic assembly using motor torques, *Proc. of 2014 IEEE International Conference on Automation Science and Engineering* (2014) 1252-1257.
[33] M. Linderoth, A. Stolt, A. Robertsson and R. Johansson, Robotic force estimation using motor torques and modeling of low velocity friction disturbances, *Proc. of 2013 IEEE/RSJ International Conference on Intelligent Robots and Systems* (2013) 3550-3556.
[34] F. Pique, M. N. Boushaki, M. Brancadoro, E. De Momi and A. Menciassi, Dynamic modeling of the da Vinci research kit arm for the estimation of interaction wrench, *Proc. of 2019 International Symposium on Medical Robotics* (2019) 1-7.
[35] J. Hollerbach, W. Khalil and M. Gautier, Model identification, *Springer Handbook of Robotics,* Springer, Cham. (2016) 113-138.
[36] J. Jovic, A. Escande, K. Ayusawa, E. Yoshida, A. Kheddar and G. Venture, Humanoid and human inertia parameter identification using hierarchical optimization, *IEEE Transactions on Robotics*, 32 (3) (2016) 726-735.
[37] R. Waiboer, Dynamic modelling, identification and simulation of industrial robots, *Doctoral Dissertation*, University of Twente, Netherlands (2007).
[38] B. Siciliano, L. Sciavicco, L. Villani and G. Orioli, *Robotics: Modelling, Planning and Control,* Springer Science & Business Media (2010).
[39] B. Armstrong-Helouvry, *Control of Machines with Friction,* Springer Science & Business Media (2012).
[40] M. Gautier, Numerical calculation of the base inertial parameters of robots, *Journal of Robotic Systems*, 8 (4) (1991) 485-506.
[41] Stäubli Faverges, *Arm - RX Series 160 Family Instruction Manual*, Faverges, France (2008).
[42] S. Diamond and S. Boyd, CVXPY: a python-embedded modeling language for convex optimization, *The Journal of Machine Learning Research*, 17 (1) (2016) 2909-2913.
[43] R. E. Perez, P. W. Jansen and J. R. R. A. Martins, pyOpt: a python-based object-oriented framework for nonlinear constrained optimization, *Structural and Multidisciplinary Optimization*, 45 (1) (2012) 101-118.

Omer Faruk Argin received the B.Sc. degree in Mechatronics Engineering from the Kocaeli University, Kocaeli, Turkey, in 2009, and the M.Sc. degree in Mechatronics Engineering from the Istanbul Technical University, Istanbul, Turkey, in 2014. He is currently a Ph.D. student at the Istanbul Technical University, Istanbul, Turkey.

Zeki Yagiz Bayraktaroglu received the B.Sc. degree in Mechanical Engineering from the Istanbul Technical University, Istanbul, Turkey, the M.Sc. in Robotics from the Ecole Nationale Supérieure d'Arts et Métiers, Paris, France and the Ph.D. in Robotics from the University of Versailles Saint Quentin-en-Yvelines, Versailles, France, in 1997, 1998, and 2002, respectively. He is currently an Associate Professor, Department of Mechanical Engineering, Istanbul Technical University.